Princeton Plasma Physics Laboratory

PPPL-5075

PPPL-5075

Advances in the Understanding of ELM Suppression by Resonant Magnetic Perturbations (RMPs) in DIII-D and Implications for ITER

R. Nazikian, D. Eldon, T.E. Evans, N.M. Ferraro, B.A. Grierson, R.J. Groebner, J.D. King, E. Kolemen, N. Logan, G.R. McKee, O. Meneghini, R.A. Moyer, D.M. Orlov, T.H. Osborne, C. Paz-Soldan, C.C. Petty, T.L. Rhodes, W.M. Solomon, O. Schmitz, M.W. Shafer, S.P. Smith, P.B. Snyder, E.J. Strait, and M.R. Wade

October 2014

PPPL PRINCETON PLASMA PHYSICS LABORATORY

Prepared for the U.S. Department of Energy under Contract DE-AC02-09CH11466.

Princeton Plasma Physics Laboratory
Report Disclaimers

Full Legal Disclaimer

Trademark Disclaimer

PPPL Report Availability

Princeton Plasma Physics Laboratory:

http://www.pppl.gov/techreports.cfm

Office of Scientific and Technical Information (OSTI):

http://www.osti.gov/scitech/

Related Links:

U.S. Department of Energy

Office of Scientific and Technical Information

Advances in the Understanding of ELM Suppression by Resonant Magnetic Perturbations (RMPs) in DIII-D and Implications for ITER

R. Nazikian 1), D. Eldon 2), T.E. Evans 3), N.M. Ferraro 3), B.A. Grierson 1), R.J. Groebner 3), J.D. King 4), E. Kolemen 1), N. Logan 1), G.R. McKee 5), O. Meneghini 3), R.A. Moyer 2), D.M. Orlov 2), T.H. Osborne 3), C. Paz-Soldan 3), C.C. Petty 3), T.L. Rhodes 6), W.M. Solomon 1), O. Schmitz 5), M.W. Shafer 7), S.P. Smith 3), P.B. Snyder 3), E.J. Strait 3), and M.R. Wade 3)

1) Princeton Plasma Physics Laboratory, Princeton, New Jersey 08543-0451, USA
2) University of California San Diego, La Jolla, California 92093-0417, USA
3) General Atomics, San Diego, California 92186-5608, USA
4) Oak Ridge Institute for Science Education, Oak Ridge, Tennessee 37830, USA
5) University of Wisconsin, Madison, Wisconsin 53706, USA
6) University of California Los Angeles, Los Angeles, California 90095-7099, USA
7) Oak Ridge National Laboratory, Oak Ridge, Tennessee 37831, USA
email: rnazikian@pppl.gov

Abstract Experiments on DIII-D have expanding the operating window for RMP ELM suppression to higher q95 with dominant electron heating and fully noninductive current drive relevant to advanced modes of ITER operation. Robust ELM suppression has also been obtained with a reduced coil set, mitigating the risk of coil failure in maintaining ELM suppression in ITER. These results significantly expand the operating space and reduce risk for obtaining RMP ELM suppression in ITER. Efforts have also been made to search for 3D cause of ELM suppression. No internal nonaxisymmetric structure is detected at the top of the pedestal, indicating that the dominant effect of the RMP is to produce an n=0 transport modification of the profiles. Linear two fluid MHD simulations using M3D-C1 indicate resonant field penetration and significant magnetic stochasticity at the top of the pedestal, consistent with the absence of detectable 3D structure in that region. A profile database was developed to compare the scaling of the pedestal and global confinement with the applied 3D field strength in ELM suppressed and ELM mitigated plasmas. The EPED pedestal model accurately predicts the measured pedestal pressure at the threshold of ELM suppression, increasing confidence in theoretical projections to ITER pedestal conditions. Both the H-factor (H98y2) and thermal energy confinement time do not degrade substantially with applied RMP fields near the threshold of ELM suppression, enhancing confidence in the compatibility of ITER high performance operation with RMP ELM suppression.

Introduction The suppression of edge localized modes (ELMs) is a requirement for high fusion power discharges in ITER. In order to address this risk posed by ELMs, various methods are being developed to substantially weaken or entirely eliminate ELMs in tokamaks [1]. One method developed first on DIII-D [2] and applied to the ITER design [3] is the use of Resonant Magnetic Perturbations (RMPs). These fields, applied by in-vessel current carrying coils (I-coils), have the potential to eliminate [2,4,5] or substantially weaken [6,7] ELMs. However both the operating space achieved using RMP ELM suppression and the physics understanding of the suppression mechanism required for extrapolation to fusion reactors need to be improved. Significant progress has been made on DIII-D in extending the operating space for RMP ELM suppression. Expansion to high $q95$ plasmas with and large fraction of electron heating and dominant noninductive current drive opens up new directions for steady state research with RMP ELM suppression. Additional windows have been opened at $q95$=4.1 with n=2 fields, allowing the investigation of advanced inductive regimes with reduced plasma current. New studies indicate that coil failure is not an impediment to achieve robust ELM suppression, reducing risk for ITER. A major concern for a reactor is main ion dilution from impurity accumulation and radiative collapse. Experiments have shown that for plasmas with well matched pedestal density, impurity accumulation is not worse for RMP ELM suppressed plasmas than for typical Type-I ELMing H-mode plasmas on DIII-D, further validating RMP ELM suppression regimes for ITER. While all these results lend confidence for effective ELM suppression in ITER high performance scenarios, a first principles physics model is still required for reliable extrapolation. Studies aimed at detecting islands at the top of the H-mode pedestal in DIII-D have yielded no clear evidence for islands. However, linear two-fluid MHD simulations clearly indicate strong

stochastization at the top of the pedestal and such fields will have the effect of shrinking islands and washing out 3D structure, consistent with the dominant observation of an n=0 transport response in ELM suppressed plasmas. Another focus of recent studies has been to quantify the energy confinement scaling and pedestal pressure scaling of plasmas with applied RMP fields. The result of these studies is that global energy confinement does not degrade substantially near the threshold of ELM suppression relative to comparable ELMing H-mode plasmas. These developments improve prospects for achieving high-performance ITER plasmas with robust ELM suppression.

2. Expansion of RMP ELM Suppression Operating Space The latest experimental campaign on DIII-D has opened up new directions for investigating ELM suppression in advanced operating regimes relevant for ITER and beyond. Steady state operation requires high safety factor to achieve high bootstrap fraction and q_{min}>2 to avoid the most deleterious MHD instabilities such as neoclassical tearing modes (NTMs), and also requires significant direct electron heating and low collisionality for efficient current drive. A target plasma matching a number of these key requirements has been achieved in DIII-D with odd parity n=3 applied RMP (upper and lower I-coils 180 degrees out of phase). The result is shown in Fig. 1(a,b) with q_{min}≈1.8, q_{95}≈6.1, β_N≈2, pedestal density close to $3x10^{19}$ m^{-3} and electron collisionality ν_e^*≈0.3. Other discharge parameters are: B_T=+2 T (reverse B_T), I_p=1.0 MA, δ_u=0.73, δ_l=0.36, κ=1.82, R=1.75 m, a=0.58 m, P_{NBI}≈9 MW. Robust ELM suppression is obtained when the I-coil current is raised to 4 kA late in the discharge after 3 s, accompanied by about a 25% reduction in the plasma density (called density pump-out).

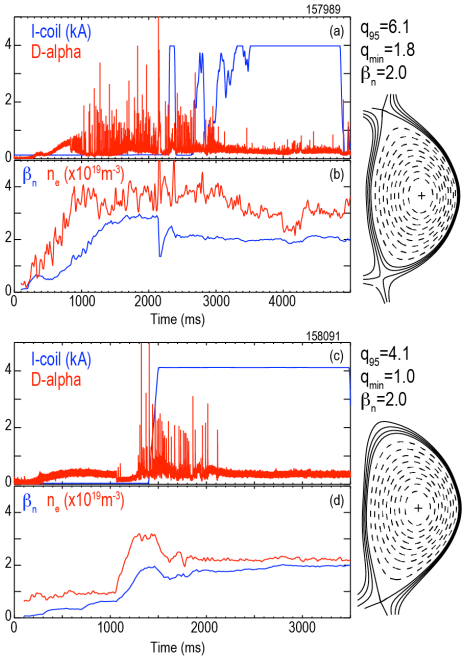

Fig. 1. (a,b) n=3 odd parity I-coil configuration with q_{95}=6.1, USN and (c,d) n=2 even parity I-coil configuration with q_{95}=4.1, LSN.

While a fusion reactor requires steady-state operation, advanced inductive (AI) regimes may be attractive for ITER to increase pulse length and achieve high fusion gain with reduced plasma current, mitigating disruption risk. For the first time, DIII-D has achieved sustained ELM suppression at q_{95}=4.1 in the ITER Similar Shape (ISS) in stationary conditions as shown in Fig. 1(c, d). Relevant discharge parameters are: B_T=-1.9 T, I_p=1.36 MA, δ_u=0.33, δ_l=0.69, κ=1.82, R=1.75, a=0.59, P_{NBI}= 6 MW, P_{EC}= 1.0 MW. Interestingly, this was accomplished with even parity n=2 RMP fields (upper and lower I-coils in phase). ELM suppression with even parity n=2 RMP was routinely achieved in the past at q_{95}=3.6 [8], suggesting n=2 islands at the top of the pedestal may also play a role in suppression.

These new results at higher q95 opened up the opportunity to explore the compatibility RMP ELM suppression with fully noninductive Hybrid plasma at q95≈6. Noninductive Hybrid plasmas are achieved using central ECCD and neutral beam heating with a central safety factor maintained above unity by anomalous poloidal flux pumping due to m/n=3/2 or 4/3 NTM activity [9]. A key question is whether hybrid plasmas can be sustained in steady state with strong ELM mitigation or complete ELM suppression. Figure 2 shows a Hybrid plasma with the ITER Similar Shape as in Fig 1b but with q95=6.5, Ip=0.95

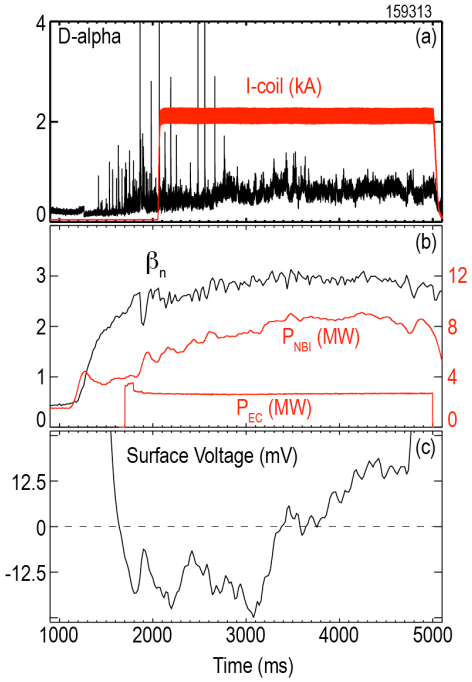

Fig. 2. Noninductive Hybrid plasma with clamping of Ohmic induction coil from 3-5 s in ISS plasma and q95=6.5.

MA, and using n=3 odd parity RMP with the I-coil. ELM suppressed hybrid plasmas were obtained with the ohmic transformer turned off from 3-5 s with peak βn=2.9 and H98y2=1.3. The plasma current (0.95 MA) and normalized internal inductance were steady during the duration of the peak NBI power with an estimated ohmic current < 40 kA (i.e., 96% noninductive current), which is in line with current drive calculations and the value of the surface loop voltage (Fig. 2c) around 3.8 sec.

An important advance on DIII-D in the last campaign was the demonstration of effective ELM suppression with a reduced coil set. Out of the 12 available I-coils (6 upper and 6 lower), ELM suppression was obtained with as few as 5 I-coils in the standard ISS plasma with q_{95}≈3.5 in ISS plasmas as in Fig. 1(c, d) but using even parity *n*=3 I-coils [10]. The dominant difference in the applied spectrum per unit kA was the addition of an *n*=1 sideband with the removal of some of the I-coils. Stable plasma operation requires the elimination of the *n*=1 sideband resulting from the removal or loss of coils. This *n*=1 sideband couples to the n=1 external kink mode, leading to locked modes. Figure 3 demonstrates this effect for two discharges, both using seven I-coils for ELM suppression. In one case (black) the induced *n*=1 sideband is optimally corrected with the external C-coils, while for the other case (red) only standard *n*=1 EF correction is used. This discharge ends in a disruption, due to a rapidly growing pre-locked *n*=1 mode, i.e., the *n*=1 mode grows in phase with the *n*=1 sideband as shown in Fig. 2c. The n=1 sideband control resulting from coil failure will likely be even more important in the low-input torque conditions on ITER.

In these experiments a clear reduction was observed in the applied *n*=3 resonant field amplitude required for ELM suppression with decreasing coil number. This suggests that other sidebands (*n*=1,2,4,…) introduced by coil removal contribute to ELM suppression. Figure 4(a) demonstrates a density threshold at the top of the pedestal for the onset of ELM suppression, independent coil number. In these experiments the pedestal density threshold for ELM suppression is close to 2.5×10^{19} m^{-3}. One possible explanation is that resonant field penetration requires a critical density (perhaps related to the parallel viscosity for island penetration). Figure 4(b) demonstrates the advantage of operating with fewer I-coils in terms of power requirements. The inverse of the I-coil current applied to each available coil is shown vs. the coil number. For 5 coils, ELM suppression is obtained with 4.5 kA current, while for 11 coils, suppression was obtained for 2.6 kA current. As the shape of the poloidal spectrum for the *n*=3 field does not change as the number of coils decreases, the *n*=3 field strength is simply proportional to the I-coil current x number of coils, representing roughly a 25% reduction in the applied *n*=3 field strength going from 11 coils to 5 coils. If we take the linear trend in the data and extrapolate to fewer coils, we can predict that ultimately,

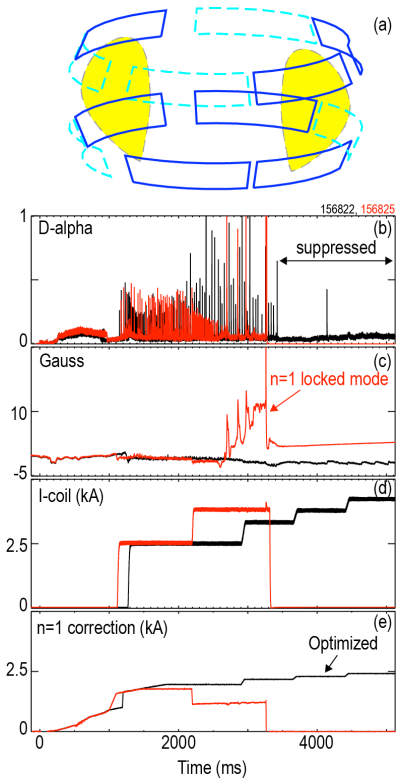

Fig. 3. (a) ELM suppresion with reduced (7) coil set on DIII-D, (b-e) waveforms for optimal *n*=1 error field correction (black) and standard erorr field correction (red) without compensation for the *n*=1 EF introduced by the removal of 5 I-coils.

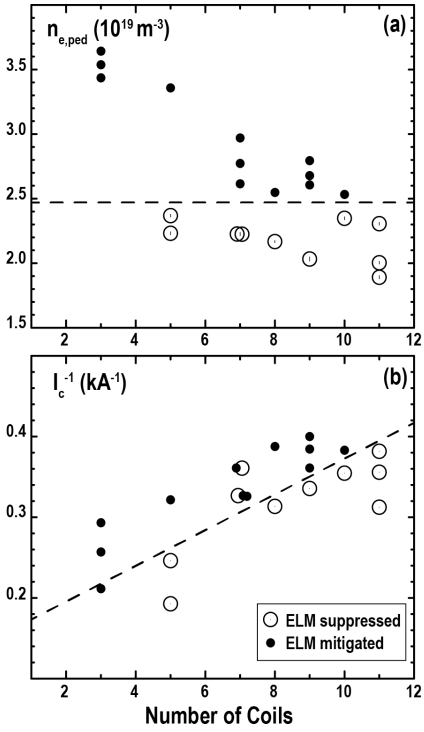

Fig. 4. (a) pedestal density vs number of active I-coils, and (b) inverse of I-coil current vs number of active I-coils. Open circles are ELM suppressed, closed circles are ELM

ELM suppression could be achieved with only one coil operating with at least 6 kA of current. However, such extrapolations should be taken with caution as the plasmas with three I-coils did not see significant density pumpout and hence could not access the density threshold for ELM suppression.

Another important advance in the last run campaign came in the area of impurity accumulation studies in plasmas with applied RMPs, again in the standard ISS plasma as in Fig. (1c, 1d) but with n=3 even parity I-coil field. Initial results suggested that at the threshold of RMP ELM suppression, higher impurity accumulation occurred for both carbon and nickel relative to the target ELMing H-mode plasma before the application of the RMP. However, these plasmas also had significant density pumpout induced by the n=3 field that led to a rise in the ion temperature at the separatrix and most likely to a rise in the carbon sputtering rate and impurity influx. When density feedback was used with deuterium gas to maintain constant pedestal density during ELM suppression, then no adverse accumulation of impurities was observed in RMP plasmas as compared to similar density ELMing H-mode plasmas. Figure 5 shows two discharges, one without n=3 RMP and one with a staircase n=3 RMP waveform and density feedback to maintain constant density at the top of the pedestal. The discharge without density feedback and without RMP (black) is compared to one with density feedback and n=3 RMP (red). The pedestal densities are closely matched [Fig. 5(b)] for the two cases. Figure 5(c) shows that the Z_{eff} from carbon is no worse in the ELM suppressed plasma than for the ELMing H-mode plasma. Figure 5(d) shows the ratio of the nickel line intensity to the electron density in the plasma core, indicating no adverse accumulation of nickel when transitioning into ELM suppression. These results bode well for RMP ELM suppression in fusion reactors by demonstrating that no adverse effect on impurity accumulation is observed in the transition to suppression.

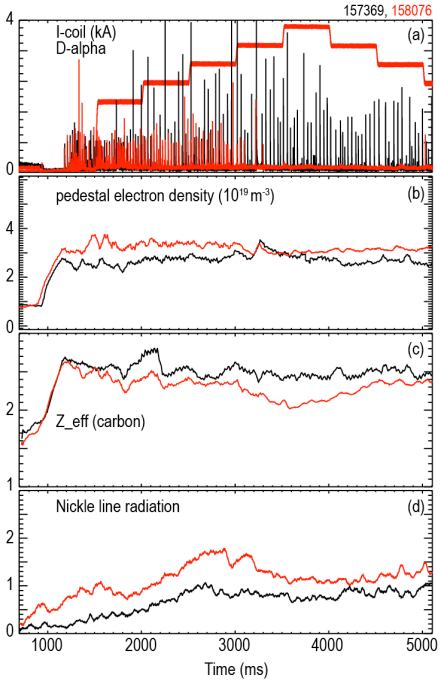

Fig. 5. (a) I-coil waveform with n=3 even parity RMP, and D_α signal for ELM suppressed plasma (red) and no applied RMP (black), (b) pedestal density, (c) Carbon Z-effective and (d)

3. Physics Advances in RMP ELM Suppression What is missing for reliable extrapolation to ITER is a validated first principles physics basis for ELM suppression. The leading model for RMP ELM suppression posits that resonant fields penetrate the plasma, opening islands at low order rational surfaces that prevent the expansion of the pedestal to an unstable width [11]. Resonant field penetration is predicted to occur where the perpendicular electron flow goes through zero according to linear two-fluid MHD calculations [12]. For ISS plasmas, this is typically near the top of the H-mode pedestal for co-I_p rotating plasmas. Islands at the top of the pedestal should have the effect of enhancing transport and preventing the expansion of the pedestal. Unfortunately, such islands are predicted to be quite narrow and perhaps at the limit of the resolution of our diagnostic capabilities. On the other hand, near the plasma edge where multiple low-order rational surfaces are in close proximity, it is theoretically predicted that substantial island overlap can occur, creating regions of radially extended stochasticity and breaking up or shrinking the magnetic islands. In such a system the dominant effect of stochasticity will be to induce an n=0 transport response of the plasma rather than clearly discernable islands.

Experiments on DIII-D attempted to identify islands by performing phase flips of the applied n=3 RMP field in ISS plasmas. This approach attempts to sweep the islands or the nonaxisymmetric plasma response across the Thomson scattering diagnostic that is located at a fixed toroidal angle. By performing multiple phase flips, we can build up statistics of the temperature profiles for two toroidal phases of the applied n=3 field separated by 180 degrees in toroidal angle. If the X (or O)-point of an

island is close to the Thomson scattering location then the phase flip will move the island such that the Thomson measurement will be located at the O (or X)-point after the flip, respectively.

A key requirement of this experiment is to eliminate n=0 line density and temperature modulation induced when the toroidal phase of the n=3 RMP field is changed. By adding an n=3 offset and flipping the sign of the I-coil current in intervals of 100 or 200 ms, we succeeded in eliminating the n=0 modulation in the density and stored energy. Figure 6(a) shows the D_α light for a phase flip experiment. The ELMs are suppressed for the most part except during the phase flips when the amplitude of the I-coil current goes through zero. A linear n=3 offset ramp is applied on the I-coils and the perturbed line density is shown relative to the I-coil current in Fig. 6(b). The perturbed density goes through zero and then reverses sign as the offset is scanned. The offset current where the density perturbation is minimized is ≈500 A. This was then applied as a constant offset in order to look for islands. Figure 6(c) shows that the line average density and β_N are minimally perturbed at the optimal offset.

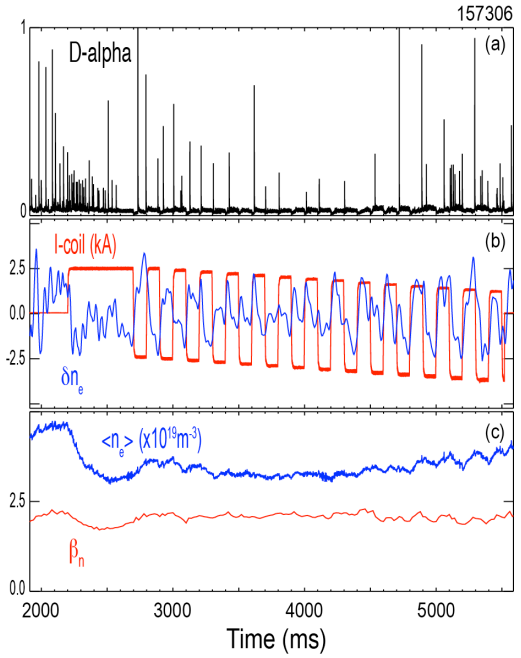

Fig. 6. (a) D_α signal, (b) I-coil waveform (red), perturbed pedestal density (blue), (c) average line density (blue) and normalized beta β_N (red).

Figure 7 shows the electron temperature profiles for an ISS discharge with q_{95}=3.5 inside the window of ELM suppression and with a train of n=3 phase flips in the I-coils. The optimal n=3 offset of 500 A is applied to the I-coil current. This leads to an I-coil current square wave with limits of -3.3 kA (standard phase) and +4.3 kA (180 deg. phase shift). Figure 7 shows two Thomson scattering electron temperature profiles overlaid for each sign of the I-coil current, shown in red and blue. The two profiles are each a summation of data in five time windows of the same phase. The error bar is the standard deviation of the measurement around the mean and the raw data is shown in the background. Averages are taken over five 200 ms durations in each toroidal phase. There is essentially no discernable difference between the profiles in the two toroidal phases. One possibility is that the measurement is not near the O or X point of the island, hence reducing the expected difference between the profiles. However, vacuum field calculations indicate that the measurement is near such an O (X) point. On the other hand, the extent of the islands is at most ±0.03 in poloidal flux from vacuum analysis. This could be measurable in the absence of stochasticity. However, as we shall see there is predicted to be significant island overlap between rational surfaces and this will tent to shrink the radial extent of the surviving island features.

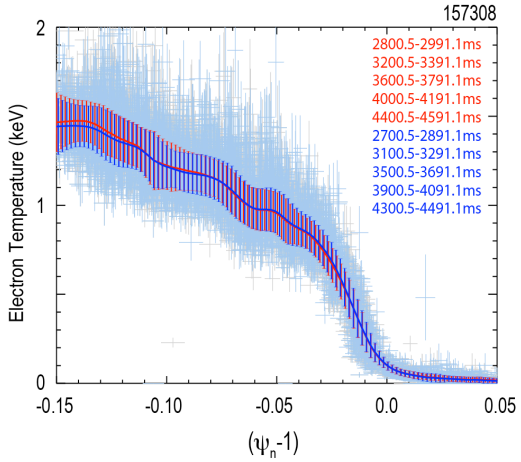

Fig. 7. Electron temperature profile averaged over multiple time windows for one toroidal phase of the n=3 even parity RMP with optimal offset applied. (red) for normal I-coil toroidal phase, (blue) for 180 deg phase toroidal phase shift.

Figure 8 shows the result of M3D-C1 simulations of the plasma response to an applied even parity n=3 RMP in the ISS plasma in Fig. 7. The I-coil current is set to 3.8 kA to take into account the 500 A offset, (average of 4.3 and 3.3 kA). The simulations show two key features compared to the vacuum field model (dotted). Figure 8(a) shows the n=3 resonant amplitude per kA of applied field at low order rational surfaces from two-fluid linear M3D-C1 simulations (solid) compared to the

vacuum field strength. The resonant field strength exceeds the vacuum field only at the top of the pedestal where the perpendicular electron velocity goes through zero whereas in the steep pressure gradient region of the pedestal at larger radius the resonant field strength is much less than vacuum, indicating effective screening. Figure 8(b) shows the Chirikov parameter exceeding unity between the rational surfaces at the top of the pedestal, indicating strong stochasticity should occur between surfaces with the result that *the islands should shrink to less than the spacing of the rational surfaces*. It is unlikely that a single island could occur with a width greater than the separation of the rational surfaces, or about Wψ≈0.04. In addition, islands can only be resolved on the temperature profile if the parallel transit time across the island is much faster than the cross-field transport. For narrow islands, this is less likely than for large islands, so that the net effect of stochasticity and the narrowing of islands is to make the direct detection of these structures extremely difficult. The result is consistent with experiment, namely a dominant *n*=0 modification of the temperature profile induced by resonant field penetration. In order to overcome these measurement limitations, other techniques will need to be developed such as heat pulse propagation or obtaining ELM suppression in limiter plasmas where the edge magnetic shear is reduced, increasing the spacing between islands.

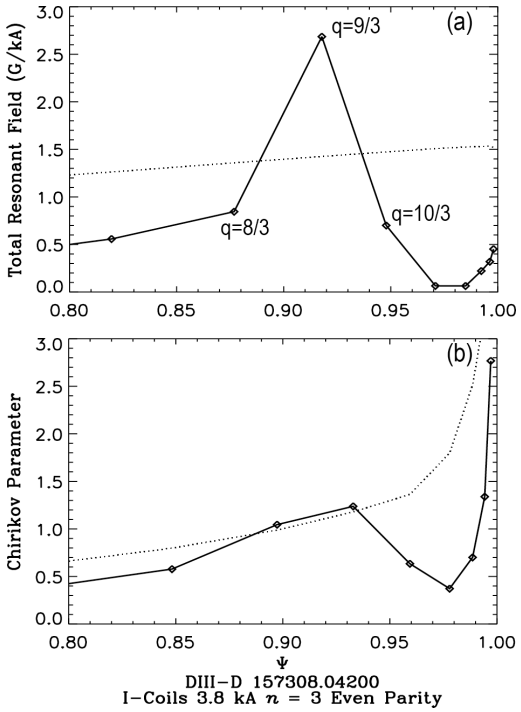

Fig. 8. M3D-C1 simulation of (a) *n*=3 resonant field amplitude on rational surfaces and (b) Chirikov parameter evaluated between rational surfaces. Vacuum field is the dotted line.

A key theoretical prediction of magnetic stochasticity induced transport is that the electron thermal diffusivity should scale as $(\delta B/B)^2$ where δB is the nonaxisymmetric field strength. For a constant heat flux through the edge plasma this would suggest that the electron temperature scale length should vary as $L_{Te} \sim (\delta B/B)^2$ at the top of the pedestal. A systematic scan of the I-coil current in ISS plasmas with constant heating power reveals such a scaling, but with an offset, as shown in Fig. 9. Figure 9 shows the scale length of T_e, n_e, p_e in normalized toroidal flux (ρ) at the top of the H-mode pedestal centered at ρ=0.92, plotted as a function of the applied I-coil current for plasmas that are ELM suppressed. Interestingly, at high I-coil current, well above suppression, the scaling is clearly quadratic with I-coil current, however near the threshold of suppression the scaling is constant. These results are consistent with stochastic field line induced transport at the top of the pedestal at high I-coil current. However it should be noted that other transport models such as flutter transport [13] are also expected to exhibit a similar quadratic dependence.

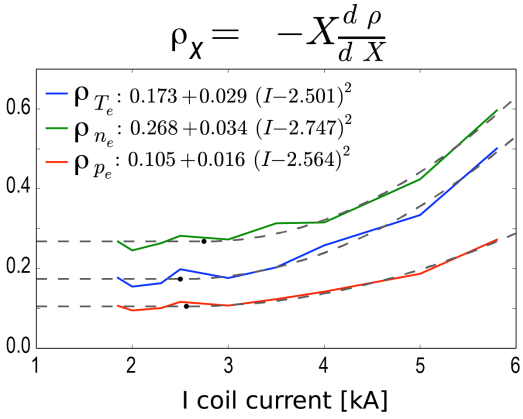

Fig. 9. Scale length in ρ of Te, ne, Pe vs I-coil current for ELM suppressed plasmas with n=3 RMP fields, centered at ρ=0.92.

4. Predictive modeling Developing a first principles physics model of ELM suppression is an essential step towards predicting performance in a future fusion reactor. However, at present such a model is still developmental. In parallel to these fundamental studies, we must also explore the scaling properties of ELM suppressed plasmas in order to perform extrapolations based on existing predictive and empirical models of the pedestal and global confinement. Two such models that are successful in predicting pedestal properties and global confinement are the EPED model and the ITER

H_{98y2} scaling of energy confinement. Figure 10 shows the result of extensive analysis of ISS plasmas for ELM-mitigated and ELM-suppressed plasmas. The electron collisionality is typically between 0.2–0.4 for all these discharges. The dominant effect of the applied n=3 RMP is on the pedestal density (density pump-out), with only a weak effect on the pedestal temperature [Fig. 10(a)]. As a consequence, the pedestal pressure (or normalized beta of the top of the pedestal) scales almost linearly with the pedestal density [Fig. 10(b)]. We can also see a well-defined density threshold for ELM suppression, close to that seen in Fig. 4. Extensive kinetic equilibrium studies on these discharges enables detailed comparison to EPED predictions. EPED is a theory based predictive model where the peeling mode stability limit determines, in combination with KBM stability, the height and width of the pedestal [11]. A comparison of the predicted pedestal height to the measured pedestal pressure is shown in Fig. 11. The vertical axis is the total measured pedestal pressure whereas the horizontal axis is the EPED model prediction. A remarkable result is that at the threshold of ELM suppression (corresponding to the points with the highest density in ELM suppression – (open circles in Fig. 10) the EPED prediction is not more than 10% higher than the measured pedestal pressure. The ELM mitigated plasmas are almost right on the EPED prediction while the ELMing H-mode cases sit somewhat above the prediction by about 10%–15%. The accuracy of the EPED model prediction is good news for predicting the pedestal height in ELM suppressed ITER plasmas. It appears that optimal pedestal pressure is achieved near the threshold of suppression and the pressure can fall well below the EPED prediction if the density is well below threshold.

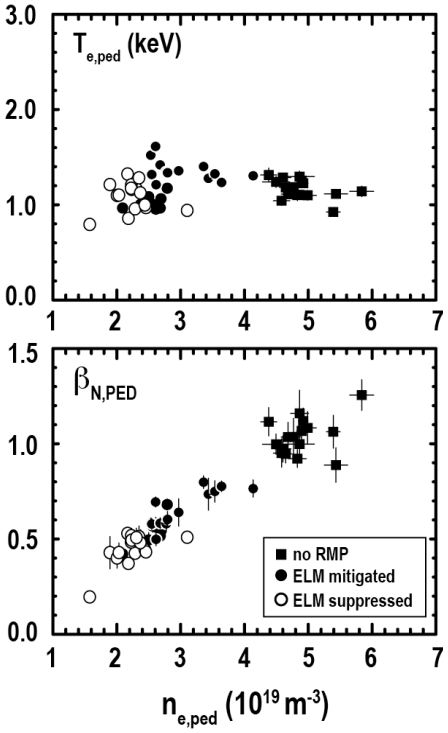

Fig. 10. (a) pedestal electron temperature, (b) pedestal beta normal for ELM suppressed (open circle), ELM mitigated (closed circle) and ELMing plasmas with no RMP. Standard ISS plasmas with n=3 even parity RMP.

Figure 12 displays the thermal energy confinement time in these plasmas vs. the pedestal density. Note there is perhaps no more than a 10% degradation of the energy confinement time for plasmas near the threshold of ELM suppression. However, the confinement can rapidly drop if the plasma is overdriven as can be seen from the low range of the ELM-suppressed confinement times in Fig. 12. A modest ~10% reduction in confinement is all that is needed to have the effect of controlling the fusion burn (Ref. [14]) and the good global confinement of these plasmas near the threshold of ELM suppression bodes well for achieving high fusion gain with ELM suppression in ITER.

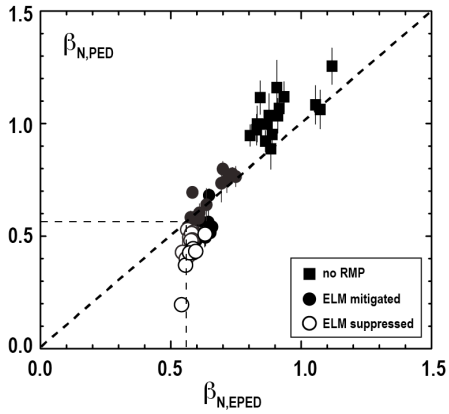

Fig. 11. Normalized pedestal beta (vertical axis) vs the EPED prediction for the data in Fig. 10.

Figure 13 shows a plot of the H-factor (H_{98y2}) on the vertical axis vs. the pedestal density for the data set in Fig. 10. The ELMing H-mode ISS plasmas (black squares) have an average H-factor of 1.1. It is interesting that the ELM mitigated plasmas at high density (filled circles) and ELM-suppressed plasmas near threshold conditions (open circles) are all close to the H-factor of the ELMing H-mode plasmas without applied RMP. We also see that the H-factor can fall well below unity but these are for plasmas that are typically overdriven, with an I-coil current significantly exceeding that required for obtaining threshold conditions for ELM suppression. The net result, based on global confinement scaling (Fig. 13) and impurity measurements (Fig. 5) is that empirically, RMP ELM suppressed plasmas should project favorably to high performance ITER conditions.

5. Summary and future directions In these proceedings we have reviewed recent progress in RMP ELM-suppression research on the DIII-D tokamak. Advances in operating space enable opportunities to explore ELM suppression in advanced operating regimes relevant to ITER. Fully noninductive current Hybrid plasmas have been achieved with suppressed ELMs. Other steady state regimes will be explored in the future. Impurity analysis indicates that low and high-Z impurity accumulation is not worse for ELM suppressed plasmas than for ELMing H-mode plasma. Empirical scaling demonstrates that global confinement is not significantly degraded at the threshold of ELM suppression. The EPED pedestal model also works surprisingly well in predicting the pedestal pressure at the threshold of suppression. These results are encouraging for ITER and suggest that ITER performance goals can be met with RMP ELM suppression. In terms of a first principles physics model, resonant field penetration and island overlap are the leading candidates to explain the phenomenon of ELM suppression. The observed scaling at the top of the pedestal is consistent stochasticity field induced transport. However new experiments will need to explore this physics mechanism in detail in order to validate advanced simulation models of resonant field penetration and rule out competing models that also exhibit similar scaling with the applied field strength.

This material is based upon work supported in part by the U.S. Department of Energy, Office of Science, Office of Fusion Energy Sciences, using the DIII-D National Fusion Facility, a DOE Office of Science user facility, under Awards DE-FC02-04ER54698, DE-AC02-09CH11466, DE-FG02-07ER54917, DE-FG02-89ER53296, DE-FG02-08ER54999, DE-FG02-08ER54984, and DE-AC05-00OR22725.

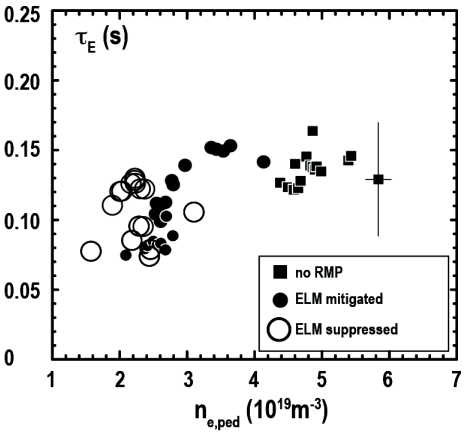

Fig. 12. Thermal energy confinement time for the data in Fig. 10.

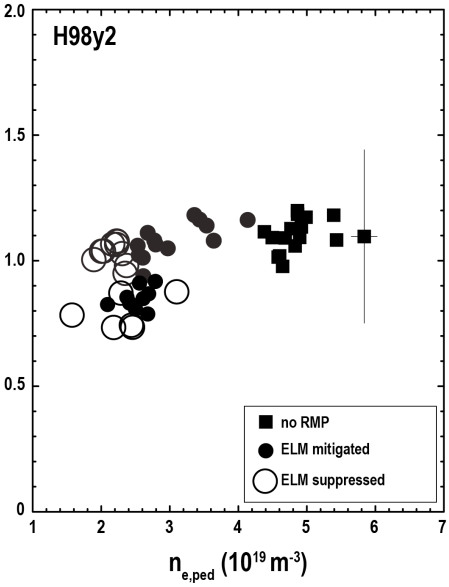

Fig. 13. Confinement factor H_{98y2} vs pedestal density for the data of Fig. 10.

References

[1] LOARTE, A., et al., Nucl. Fusion **54** (2014) 033007
[2] EVANS, T.E., et al., Nature Physics **2** (2006) 419
[3] EVANS, T.E., et al., Nucl. Fusion **53** (2013) 093029
[4] JEON, Y.M., et al., Phys. Rev. Lett. **109** (2012) 035004
[5] SUTTROP, W., et al., Phys. Rev. Lett. **106** (2011) 225004
[6] KIRK, A., et al., Nucl. Fusion **50** (2010) 034008
[7] LIANG, Y., et al., Nucl. Fusion **53** (2013) 073036
[8] LANCTOT, M.J., et al., Nucl. Fusion **53** (2013) 083019
[9] PETTY, C.C., et al., Nucl. Fusion **50** (2010) 022002
[10] ORLOV, D.M., et al., these proceedings
[11] SNYDER, P.B., et al., Phys. Plasmas **19** (2012) 056115
[12] WADE, M.R., et al., "Advances in Physics Understanding of ELM Suppression Using Resonant Magnetic Perturbations in DIII-D," submitted to Nucl. Fusion (2014)
[13] CALLEN, J.D., et al., Nucl. Fusion **53** (2013) 113015
[14] HAWRYLUK, R.J., et al., these proceedings

Princeton Plasma Physics Laboratory
Office of Reports and Publications

Managed by
Princeton University

under contract with the
U.S. Department of Energy
(DE-AC02-09CH11466)

P.O. Box 451, Princeton, NJ 08543
Phone: 609-243-2245
Fax: 609-243-2751

E-mail: publications@pppl.gov
Website: http://www.pppl.gov